

Polar domain fluctuations in doped liquid nitrobenzene

David P. Shelton^{a)}*Physics Department, University of Nevada, Las Vegas, Nevada 89154-4002, USA*

(Received 27 June 2008; accepted 27 August 2008; published online 1 October 2008)

Improved spectral measurements of the narrow spike in the high resolution hyper-Rayleigh light scattering spectrum for deuterated liquid nitrobenzene ($C_6D_5NO_2$) doped with triflic acid (CF_3SO_3H) determined that the reorientation time for the dopant-induced polar domains is $2.9 \mu s$ in the dilute limit. Two models based on ions dissolved in nitrobenzene fit the measured spectral broadening function. © 2008 American Institute of Physics. [DOI: 10.1063/1.2987297]

I. INTRODUCTION

The structure of polar molecular liquids is an unsolved problem of long standing, which has recently received renewed attention in the form of theoretical calculations and model simulations.^{1–15} The structures found in simulations of model fluids include chains of head-to-tail dipoles,^{3–7} columnar ferroelectric phases,⁹ bubble domains,¹⁰ and dipoles with vortex orientational order.^{11,12,15} However, although a recent large-scale molecular dynamics simulation for water¹⁶ found a vortexlike structure of the dipole field, even more recent large-scale molecular dynamics simulations for liquid water¹⁷ and acetonitrile,¹⁸ employing realistic intermolecular interaction potentials, failed to find evidence for ferroelectric ordering of the molecules.

Experimental evidence for ferroelectric molecular order in real liquids comes from recent hyper-Rayleigh scattering (HRS) measurements for water,¹⁹ acetonitrile,²⁰ nitromethane,²¹ and nitrobenzene (NB).²² These experiments measured the spectrum of the light scattered by the liquid, near the second harmonic frequency of the incident laser beam, for several combinations of incident and scattered light polarization. A narrow spike is observed at zero frequency shift in the VH depolarized HRS spectrum (where V denotes vertical linear incident-electric-field polarization, H denotes horizontal linear scattered-electric-field polarization, and the scattering plane is horizontal). This spike is not present in the VV or HV HRS spectra, which identifies it as due to a longitudinal polar collective mode.^{20,23} The spectral width of the spike is <10 MHz, which corresponds to a relaxation time >30 ns for this mode,^{19,21,22} very long compared to the picosecond molecular reorientation time scale. This long-lived collective mode with polar molecular order is ascribed to slowly relaxing ferroelectric domains in the liquid. The main result of this work is an improved determination of the fluctuation time for the polar domains in NB, which gives information about their size and motion. Systematic errors in the spectral broadening measurements limited the accuracy of the fluctuation times obtained from the previous experiment.²² These systematic errors have been identified and eliminated in the present work.

II. EXPERIMENTAL METHOD

The experimental apparatus and procedure for measuring the high resolution VH HRS spectrum of NB are similar to those previously described.^{22,24} Linearly polarized pulses from an injection-seeded single-longitudinal-mode Nd:YAG (yttrium aluminum garnet) laser are focused onto the liquid sample contained in a 1 cm spectroscopic cuvette. Light scattered around the 90° scattering angle is collected and collimated by a numerical aperture (NA) 0.62 lens, analyzed by a polarizing beam splitter, fiber coupled to a scanning confocal Fabry–Pérot (FP) interferometer, and then fiber coupled to an interference filter and the photon counting detector. The instrument spectral response function (reference spectrum) was measured by scanning the second harmonic light generated by a potassium titanyl phosphate crystal. Several thousand scans of the reference and the HRS signal were alternated for each sample measurement. All spectra were acquired at a sample temperature of $T=27.0^\circ C$.

The apparatus and techniques employed earlier have been refined to improve the sensitivity of the line broadening measurements and to eliminate significant systematic errors. A FP interferometer with higher reflectivity mirrors and larger mirror spacing [free spectral range (FSR)=750 MHz] is used to obtain higher resolution [9 MHz full width at half maximum intensity (FWHM)], and it is hermetically sealed to eliminate the effect of barometric pressure fluctuations. The pulse-to-pulse jitter of the laser frequency has been reduced by better vibration isolation and a more rigid resonator structure, so that the time averaged linewidth for the laser is at the 3.2 MHz FWHM Fourier transform limit for the pulses. The resulting instrumental linewidth is 13 MHz FWHM including the contributions of the laser second harmonic linewidth, the FP resolution, and the drift of the laser with respect to FP scans taken during the course of the experiment.

The measured HRS spectrum is the convolution of the true HRS spectrum with the instrument spectral function, so deconvolution is required to obtain the true HRS bandwidth. A reliable result for the HRS spectral width when it is small compared to the instrument resolution requires both a strong signal to reduce statistical uncertainties and careful attention to potential systematic errors. The transmission peak for the confocal spherical FP is sensitive to the transverse distribu-

^{a)}Electronic mail: shelton@physics.unlv.edu.

tion of the light on the two interferometer mirrors due to the spherical aberration of the mirrors.^{25,26} As the spot size is increased the transmission peak shifts to lower frequency, the width increases, and the peak skews to higher frequency. Therefore, the illumination of the FP by the signal and reference light must be very carefully matched in terms of spatial and angular distributions. (Reference illumination using a too small NA accounts for most of the 3 MHz systematic error in the previous experiment.²²) The HRS light from the sample is collimated by an aspheric lens and then focused by a second aspheric lens onto the optical fiber that transmits the light to the FP. In the present apparatus a polarizing beam splitter is placed between these lenses to serve as the polarization analyzer for the HRS light and as the beam combiner for the HRS and reference beams. The image of the HRS source on the fiber input end is a thin line, and the reference beam optics are constructed to give a matching image for the reference light. An aperture stop placed before the second lens, in the common path for both beams, helps ensure that the NA is the same for both beams focused onto the fiber. Small differences between the beams coupled into the fiber are reduced by a mode scrambler consisting of a series of microbends of the fiber.²⁷ As a final precaution, the reference must be generated from the same laser beam that goes to the HRS sample cell since the beam out of the rear mirror of the slave laser is contaminated with the seed laser beam and will produce a different spectrum. The adequacy of the matching of the sample and reference illumination of the FP was tested using fused silica glass as the sample. The fused silica HRS spectrum should have zero broadening and shift compared to the reference spectrum. The fused silica HRS spectrum was fit with the peak obtained by convolving the reference spectrum with a Lorentzian function $L(\nu)=A/[1+(\nu/\nu_0)^2]$ and then shifting by $\Delta\nu$. The broadening and shift (ν_0 and $\Delta\nu$) of the fused silica HRS spectrum are both zero to within the 15 kHz statistical uncertainty of the fit.

There is one further systematic error due to weak absorption of the 1064 nm laser beam that occurs for typical liquid samples but not for fused silica. The HRS signal is produced near the focused beam waist from a volume about 6 μm diameter and 0.1 mm long in these experiments. The temperature of the liquid in this small volume will rise during the laser pulse, the refractive index n will fall, and the wavefronts of the incident laser beam will advance further than they would have. The optical phase at distance z from the start of a uniformly heated zone is $\phi(t)=\omega_L t-2\pi n z/\lambda_L$. The instantaneous frequency is $\omega(t)=d\phi/dt$, so the time variation in n due to heating causes a shift to higher frequency: $\Delta\nu/\nu_L=-(dn/dt)z/c$. The shift will vary both along the beam track and in time since the rate of rise of the temperature during the pulse is not constant. For NB the refractive index temperature coefficient²⁸ is $dn/dT=-4.6\times 10^{-4}\text{ K}^{-1}$ so a temperature rise by 1 K in 100 ns acting over a length of 0.1 mm in the liquid gives an upshift of 1 MHz. The measured laser absorption is 0.4 m^{-1} for NB so the estimated temperature rise of the focal cylinder for a 0.1 mJ pulse is 0.8 K (considering the heat capacity but ignoring the thermal conductivity of the liquid) and the estimated shift for the HRS light generated at the waist is about 0.4 MHz,

TABLE I. VH HRS measurements for NB-triflic acid solutions. The tabulated error bars are the uncertainties due to photon counting statistics added to 1% of S/B or 5% of ν_0 due to other contributions.

x	S/B ^a	ν_0 (MHz)
1.71×10^{-7}	0.019 ± 0.001	0.05 ± 0.09
1.20×10^{-6}	0.109 ± 0.002	0.08 ± 0.05
8.46×10^{-6}	0.270 ± 0.005	0.12 ± 0.03
5.97×10^{-5}	0.348 ± 0.007	0.49 ± 0.06
4.20×10^{-4}	0.379 ± 0.007	1.36 ± 0.10
2.95×10^{-3}	0.380 ± 0.009	5.44 ± 0.35
2.06×10^{-2}	0.377 ± 0.016	21.4 ± 1.4

^aSolvent $S/B=(5.9\pm 0.6)\times 10^{-3}$.

consistent with the observed upshift of about 0.3 MHz for 0.1 mJ pulses. The observed shift increases with laser beam power, and the observed broadening is less than 0.3 times the shift. Since the laser absorption is 20 times less for deuterated NB, the HRS peak shift is effectively eliminated for $\text{C}_6\text{D}_5\text{NO}_2$. The HRS signal is also increased since the thermal lens effect is greatly reduced. The experiments reported here used deuterated NB.

III. EXPERIMENTAL RESULTS

The VH HRS spectra of NB obtained in this experiment consist of a narrow peak riding on a flat background. The narrow peak is the instrumentally broadened spike. The flat background is formed from the broader components of the NB HRS spectrum by the overlap of 2400 successive spectral orders of the FP interferometer which fall within the 60 cm^{-1} bandpass of the interference filter. One FSR contains the integrated intensity of the HRS spectrum. The HRS spectrum is fitted with a function composed of a constant background term added to the peak obtained by convolving the reference spectrum with a Lorentzian function $L(\nu)=A/[1+(\nu/\nu_0)^2]$. For all spectra the Lorentzian broadening function gives an excellent fit to the data as judged by the χ^2 test. The principal results obtained from each spectrum are as follows: S/B , the ratio of the integrated intensities of the peak (S) and the background (B) and ν_0 , the spectral width of the spike.

Deuterated NB ($\text{C}_6\text{D}_5\text{NO}_2$) (Isotec, 99.5 at. % D) gave S/B in the range of 0.001–0.006 and was used as received. Samples were prepared by adding triflic acid (TfA, $\text{CF}_3\text{SO}_3\text{H}$) (Sigma-Aldrich, reagent grade) to deuterated NB, and then successively diluting this solution. Solution concentrations were determined by weighing the components, and samples were measured about 5 days after preparation.

Results of the HRS measurements are summarized in Table I and displayed in Fig. 1. Polar order of the liquid is indicated by the ratio S/B , which increases and then saturates as the mole fraction x of triflic acid dissolved in the NB increases. The variation in S/B seen in Fig. 1(a) is described by a curve of the form

$$f(x) = (S/B)_{\text{max}}[x/(x+x_0)] \quad (1)$$

with coefficients $(S/B)_{\text{max}}=0.374\pm 0.005$ and $x_0=(3.03\pm 0.11)\times 10^{-6}$ (the saturation mole fraction). The tabulated results have been corrected for the effect of the

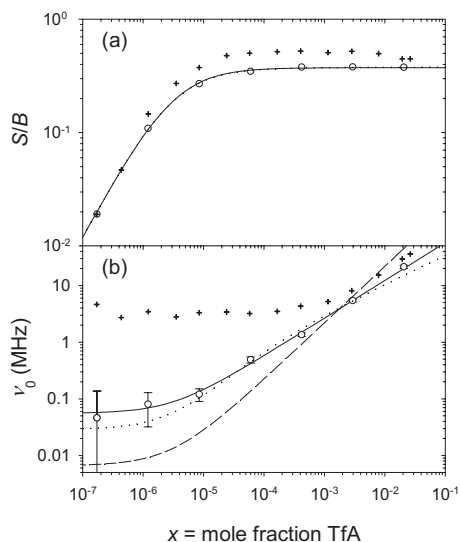


FIG. 1. VH HRS measurements for NB-triflic acid solutions plotted vs triflic acid mole fraction x . The present measurements, given in Table I, are shown as open circles, and the previous results (Ref. 22) are shown as crosses. The solid curve in (a) is the fit of Eq. (1) to the spike intensity S/B , while the solid curve in (b) is the fit of Eq. (2) to the spectral width ν_0 . The dashed curve in (b) is a plot of Eq. (4), and the dotted curves in (a) and (b) are obtained by fitting Eqs. (5)–(7) to the data.

residual impurity of the NB solvent using the expression: $S/B = (\text{solution } S/B) - (\text{solvent } S/B) / [1 + (x/x_0)^2]$. This expression assumes that the effect of the residual impurities in the NB is the same as the effect of a small added increment of acid. The previous measurements agree with the present results for low acid concentration but fall above the present results for high acid concentration. This appears to be an aging effect and is interpreted as due to restructuring of the packed domains in highly doped samples. The previous measurements were made within 1 day of sample preparation while the measurements presented here were made 5 days after sample preparation.

Figure 1(b) shows that the spectral width of the spike in the VH HRS spectrum ν_0 increases with x over the entire concentration range measured. The variation in ν_0 seen in Fig. 1(b) is described by a curve of the form

$$\nu_0(x) = \nu_m [1 + x/x_0]^{2/3} \quad (2)$$

with $\nu_m = 55 \pm 2$ kHz. The Lorentzian width ν_m for the spike at low x corresponds to an exponential relaxation time $\tau_m = (2\pi\nu_m)^{-1} = 2.9 \pm 0.1$ μs . The previous measurements of ν_0 fall about 3 MHz above the present results due to a systematic error in the previous measurements.

HRS spectra were measured for a range of laser power for the $x = 5.97 \times 10^{-5}$ sample to check that the observed spectra are intrinsic to the sample and are not induced by the laser. The results for S/B and ν_0 are independent of the average laser beam power over the range of 0.4–1.2 W (results in Table I were obtained at 0.4 W).

The intensity of the spike was measured and compared for VH and HV polarization geometries for the $x = 5.97 \times 10^{-5}$ and $x = 1.71 \times 10^{-7}$ samples. For these measurements the NA for light collection from the sample was reduced from NA=0.48 to NA=0.26 to reduce the amount of VH polarized light mixed into the HV signal. The predicted in-

tensity of the spike observed in the HV spectrum due entirely to this mixing is 11.4% of the VH spike intensity.²³ The observed HV spike intensities are $11.4 \pm 0.7\%$ and $14 \pm 3\%$ of the VH intensity for the high and low x samples, respectively. Thus, there is no detectable spike with true HV polarization for either sample. This shows that long range (280 nm wavelength) longitudinal orientation correlations persist even in the most dilute doped sample measured. For the undoped NB sample, the measured HRS integrated intensity ratios were $VV/HV = 5.4 \pm 0.1$, $HH/VH = 1.11 \pm 0.02$, and $HV/VH = 1.56 \pm 0.05$.

IV. DISCUSSION

The interpretation of the results of this experiment is that polar domains are induced and stabilized by TfA.²² It is assumed that the liquid at low dopant concentration contains isolated domains of characteristic volume V_D and the number of domains is proportional to x , while at high dopant concentration the domains fill the entire liquid volume. The characteristic volume of the domains is estimated from the dopant saturation mole fraction x_0 , assuming that at saturation each dopant molecule induces formation of a domain and the domains fill the liquid. Thus, the number of NB molecules in a domain is $M = x_0^{-1} = (3.30 \pm 0.12) \times 10^5$ molecules, occupying a volume $V_D = (5.65 \pm 0.20) \times 10^4$ $\text{nm}^3 = (38.4 \pm 0.5$ $\text{nm})^3$. The radius of spherical domains with volume V_D is $R = 23.8 \pm 0.3$ nm. This domain size estimate is 10% larger than the previous estimate²² due mostly to the differences in the S/B data.

The time scale for domain motion is experimentally determined as the relaxation time $\tau = (2\pi\nu_0)^{-1}$ and will be some function of the domain size. One model for the domain size assumes that the domain volume tends to a constant limiting value $V \rightarrow V_D$ for $x < x_0$ and becomes inversely proportional to x for dopant concentration $x > x_0$. An explicit expression for the assumed domain size variation is

$$V(x) = V_D [1 + x/x_0]^{-1}. \quad (3)$$

This volume dependence is consistent with a model where each TfA molecule dissociates to form a triflate ion (CF_3SO_3^-) that induces and stabilizes a domain. It is further assumed that the polarization direction of the domain is determined by the position of the triflate ion, and that the domain polarization reorients to follow the triflate ion as it diffuses around. Then the time scale for domain orientation fluctuation is the time it takes for the triflate ion to diffuse a distance equal to the domain radius R . Since $\tau \propto R^2$ for diffusion, and $R \propto V^{1/3}$, the broadening of the VH spectral spike due to this motion will be $\nu_0 \propto \tau^{-1} \propto V^{-2/3}$. The function with this form obtained assuming Eq. (3) for $V(x)$ is just Eq. (2), which is seen to be a good fit to the data for ν_0 , as shown in Fig. 1(b). Using $\tau_m = 2.9$ μs and $R = 23.8$ nm, one estimates the diffusion coefficient $R^2/\tau_m = 2.0 \times 10^{-10}$ m^2/s for the triflate ion in NB. This value falls near the range for other anions in NB. For comparison, the diffusion coefficient is 2.6×10^{-10} m^2/s for BF_4^- in NB (Ref. 29) and 5.7×10^{-10} m^2/s for HSO_3F^- in NB,³⁰ estimated from conductivity measurements using the Nernst–Einstein equation.

An alternative model for the domain motion is orientational diffusion of the domain as if it were a rigid spherical particle.³¹ In this case

$$\nu_0(x) = (kT/2\pi\eta V_D)[1 + x/x_0], \quad (4)$$

where $\eta = 1.78 \times 10^{-3}$ N s m⁻² at $T = 300$ K is the viscosity of liquid NB (Ref. 32) and $\nu_0(x=0) = kT/2\pi\eta V_D = 6.6$ kHz is the predicted minimum linewidth. The prediction of this model is shown as the dashed curve in Fig. 1(b) and it clearly does not fit the data. However, this model can be made to fit the data if one does not assume complete ionic dissociation of triflic acid in NB, so that the mole fraction x' of triflate ions is given by

$$x' = \frac{K}{2} \left[\left(\frac{4x}{K} + 1 \right)^{1/2} - 1 \right], \quad (5)$$

where x is the mole fraction of TfA added to the NB and K is the dissociation constant. Then S/B and ν_0 as functions of x' are given by

$$f(x') = (S/B)'_{\max} [x'/(x' + x'_0)], \quad (6)$$

$$\nu_0(x') = \nu'_m [1 + x'/x'_0]. \quad (7)$$

The dotted curves in Fig. 1 show the fit to the data for this model with coefficients $(S/B)'_{\max} = 0.378 \pm 0.004$, $x'_0 = (3.05 \pm 0.09) \times 10^{-6}$, $\nu'_m = 29 \pm 9$ kHz, and $K = (1.3 \pm 1.1) \times 10^{-4}$ ($\times 9.8$ M = 1.3 ± 1.1 mM). The curves for S/B given by Eqs. (1) and (6) are almost indistinguishable, but the curve for ν_0 given by Eq. (7) does not fit the data as well as Eq. (2). The result $\nu'_m = 29$ kHz ($\tau'_m = 5.5 \pm 1.7$ μ s) is consistent with orientational diffusion of an effective reorienting volume four times smaller than V_D (15 nm hydrodynamic radius). The dissociation constant for CF₃SO₃F in NB has not been measured but the value 1.3 mM estimated here is comparable to the measured values for other strong acids and their salts. The ionic dissociation constant in NB is 20 mM for (CH₃)₄NSO₃F, 0.5 mM for (C₆H₅)₃CBF₄, and 6 μ M for HSO₃F.^{29,30} A measurement of the dissociation constant for TfA in NB would decide between the alternative models for domain orientation fluctuations.

In summary, although the observed scattered light signal comes from the NB molecules, dissolved ions and not the direct dipolar coupling of the NB molecules appears to exert the controlling influence on the polar domain size and fluctuation time scale. Two models based on ions dissolved in NB are able to account for the spectral broadening function measured in the present experiment. Furthermore, polar domains indicated by the VH spike appear to vanish for pure

NB. If this is true in general it erases the apparent discrepancy between simulations^{17,18} and experiment¹⁹⁻²² for dipolar liquids since then both would agree on the absence of polar order in the pure liquid. This raises the question as to whether the VH spike observed in other dipolar liquids will vanish when they are de-ionized, and whether the VH spike can be induced in all other dipolar liquids by dissolved ions. The organization of the molecules in these polar domains remains to be determined.

ACKNOWLEDGMENTS

This work was supported by grant CHE-0552007 from the National Science Foundation.

- ¹J. Bartke and R. Hentschke, *Phys. Rev. E* **75**, 061503 (2007).
- ²J. Bartke and R. Hentschke, *Mol. Phys.* **104**, 3057 (2006).
- ³R. Hentschke, J. Bartke, and F. Peth, *Phys. Rev. E* **75**, 011506 (2007).
- ⁴K. Van Workum and J. F. Douglas, *Phys. Rev. E* **71**, 031502 (2005).
- ⁵S. H. L. Klapp, *J. Phys.: Condens. Matter* **17**, R525 (2005).
- ⁶V. V. Murashov, P. J. Camp, and G. N. Patey, *J. Chem. Phys.* **116**, 6731 (2002).
- ⁷P. J. Camp, J. C. Shelley, and G. N. Patey, *Phys. Rev. Lett.* **84**, 115 (2000).
- ⁸B. Huke and M. Lucke, *Rep. Prog. Phys.* **67**, 1731 (2004).
- ⁹J.-J. Weis and D. Levesque, *J. Chem. Phys.* **125**, 034504 (2006).
- ¹⁰B. Groh and S. Dietrich, *Phys. Rev. E* **53**, 2509 (1996).
- ¹¹B. Groh and S. Dietrich, *Phys. Rev. E* **57**, 4535 (1998).
- ¹²B. Groh and S. Dietrich, *Phys. Rev. Lett.* **79**, 749 (1997).
- ¹³B. Groh and S. Dietrich, *Phys. Rev. E* **55**, 2892 (1997).
- ¹⁴G. Karlstrom, *J. Phys. Chem. B* **111**, 10745 (2007).
- ¹⁵D. Lu and S. J. Singer, *J. Chem. Phys.* **103**, 1913 (1995).
- ¹⁶J. Higo, M. Sasai, H. Shirai, H. Nakamura, and T. Kugimiya, *Proc. Natl. Acad. Sci. U.S.A.* **98**, 5961 (2001).
- ¹⁷P. Kumar, G. Franzese, S. V. Buldyrev, and H. E. Stanley, *Phys. Rev. E* **73**, 041505 (2006).
- ¹⁸M. A. Pounds and P. A. Madden, *J. Chem. Phys.* **126**, 104506 (2007).
- ¹⁹D. P. Shelton, *Phys. Rev. B* **72**, 020201(R) (2005).
- ²⁰D. P. Shelton, *J. Chem. Phys.* **123**, 084502 (2005).
- ²¹D. P. Shelton, *J. Chem. Phys.* **123**, 111103 (2005).
- ²²D. P. Shelton and Z. Quine, *J. Chem. Phys.* **127**, 204503 (2007).
- ²³D. P. Shelton, *J. Opt. Soc. Am. B* **17**, 2032 (2000).
- ²⁴D. P. Shelton, *J. Chem. Phys.* **124**, 124509 (2006).
- ²⁵M. Hercher, *Appl. Opt.* **7**, 951 (1968).
- ²⁶J. M. Vaughan, *The Fabry-Perot Interferometer: History, Theory, Practice, and Applications* (Adam Hilger, Bristol, 1989).
- ²⁷S. Savovic and A. Djordjevich, *Appl. Opt.* **46**, 1477 (2007).
- ²⁸J. Timmermans, *Physico-Chemical Constants of Pure Organic Compounds* (Elsevier, New York, 1950), Vol. 1.
- ²⁹F. Mijangos, J. Iturbe, and L. M. Leon, *J. Electroanal. Chem.* **188**, 219 (1985).
- ³⁰W. Reed, D. W. Secret, R. C. Thompson, and P. A. Yeats, *Can. J. Chem.* **47**, 4275 (1969).
- ³¹M. F. Kropman, H.-K. Nienhuys, and H. J. Bakker, *Phys. Rev. Lett.* **88**, 077601 (2002).
- ³²*CRC Handbook of Chemistry and Physics*, 68th ed., edited by R. C. Weast (CRC, Boca Raton, 1987).